JOURNAL OF MATERIALS SCIENCE **39** (2004) 3577– 3586

Simulation of small-strain deformations of semi-crystalline polymer: Coupling of structural transformations with stress-strain response

V. OSHMYAN
Institute of Chemical Physics, Russian Academy of Sciences, 4 Kosygin. Str., 119991 Moscow, Russia

S. PATLAZHAN
Institute of Problems of Chemical Physics, Russian Academy of Sciences, Chernogolovka, Moscow Region 142432, Russia

Y. REMOND
Institute of Mechanics of Fluids and Solids UMR 7507 ULP CNRS, 2 rue Boussingault, F-67000 Strasbourg, France
E-mail: remond@imfs.u-strasbg.fr

The small strain (below yielding) tensile loading-unloading tests were carried out on the low-density polyethylene (LDPE) and polypropylene (PP) at low strain rate and room temperature. The experiments unambiguously indicate to a remarkable decrease in residual strains in comparison with those predicted by conventional viscoelastic models. These deviations cannot be explained without taking into account structural transformations of semi-crystalline polymers. As long as small deformations cannot result in significant change in content and texture of crystalline and amorphous components, it was assumed that such transformations should include disintegration of connectivity in crystallite clusters. This structural rearrangement is supposed to be caused by the strain-induced decrystallization of narrow (and thus highly stressed) "bridges" connecting domains of conjugated crystallites or inside crystallites. A simple 1D modelling of the deformation processes supports this expectation. The disconnection in polymer morphology is simulated by small portions of amorphous ligaments appearing between neighbouring crystallites in the course of deformation. In spite of simplicity of the model a precise fitting of the stress-strain diagram is obtained along with small variations in structural and material characteristics (crystallinity degree, effective rigidity and plastic ability) of the concerned polymers.

1. Introduction

The modern knowledge of large-strain behaviour of materials excludes any doubts in the fact that it is accompanied and influenced by structural evolution [1–3]. This general phenomenon becomes much pointed for polymer materials, especially semi-crystalline polymers (SCP), characterized by greatly intricate morphology (see, for example, [4–9]). Specifically, the large-strain drawing of SCP causes orientation of crystallites as well as of macromolecules of amorphous phase down the drawing direction and entails the appreciable strain hardening.

On the contrary, one could expect that small strains (below the yield point) would not cause noticeable changes in polymer morphology thus obeying the conventional viscoelastic behaviour (say in a framework of Maxwell model). Nevertheless, it was curious to find that even in the small strain limit SCP reveals unusual mechanical response. It becomes apparent in the low slope of the unloading branch of the stress-strain diagram then leading to the unexpectedly small value of the residual strain. Preliminary results were recently reported in [10, 11]. It is demonstrated in Fig. 1 on the example of PP. It is possible to obtain a good fitting of the loading portion of the diagram within the Maxwell model (solid line in Fig. 1). However the obtained characteristics cannot be recognized as adequate ones for the unloading part: the resulted residual strain and the slope of this curve exceed significantly the experimental values. In turn, the unloading curve also can be well fitted but by a weak Maxwell element (the dotted line in Fig. 1) having rather lower elastic modulus (E_u) and different viscosity (η_u) then those (E_l and η_l) estimated at loading. Moreover, in contrast to E_l and η_l the characteristics of unloading Maxwell element strongly depend on the strain value $\bar{\varepsilon}$ at the return point. Other classical models of viscoelasticity give practically the same result.

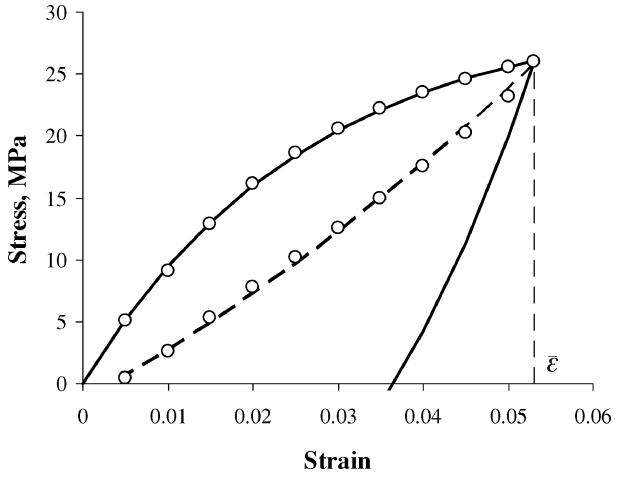

Figure 1 The loading-unloading diagrams for PP at the fixed strain rate. Open circles are the experimental data. The upper solid curve is the resultant of fitting of the loading part of the diagram by a "strong" Maxwell element with $E_{\mathrm{l}} = 1140$ MPa, $\eta_{\mathrm{l}}\dot{\varepsilon} = 30.2$ MPa. The lower solid curve represents the unloading of the same Maxwell element. The dotted curve is the fitting of the experimental unloading data by a "week" Maxwell element with $E_{\mathrm{u}} = 399$ MPa, $\eta_{\mathrm{u}}\dot{\varepsilon} = 38.6$ MPa.

Such formal analysis supports an intuitive expectation that deformation causes changing of certain part of elements caring the load and thus responsible for the viscoelastic reaction. Unloading follows the active tension. Therefore the slop (modulus) of the corresponding portion of the stress-strain diagram should be lower.

The similar quality of the small-strain behaviour of isotactic polypropylene and LDPE was recently observed by Drozdov and Christiansen [12, 13]. Interpreting this phenomenon, the authors have also explored the idea that a certain portion of deformation elements involved to the active loading becomes excluded in a process of the unloading. In contrast to the formal approach discussed, they have drawn a certain physical picture considering the semi-crystalline polymer as a network of amorphous meso-regions linked by entanglements and crystalline nodes. It was supposed that a portion of crystalline nodes crashes at unloading. This process results in a diminution of a number of active meso-regions leading to the decrease in a value of elastic modulus. The precise fitting of experimental data has been developed on the basis of this scenario. There are no doubts that idea of strain-induced structural evolution is fruitful in the interpretation of the observed phenomenon. Nevertheless, the proposed model is faced the series of objections. Three of them seem to be most important.

First, the fitting parameters of [12, 13] depend strongly upon maximum strain value $\bar{\varepsilon}$, which is the case of the cited Maxwell model. There is no physical sense in this result. Second, the crash of crystalline links was supposed to take place only at the unloading stage. But the material is exposed to the stretching (not compression!) by positive forces both at loading and unloading. Moreover, the values of the forces are higher at loading (see Fig. 1). Therefore namely the former stage should be more efficient in the structural evolution. The third objection is that it is hardly believed that sufficient change in structure parameters (in particular, the number of active meso-regions in [12, 13]) could occur in the limit of small deformations.

Nevertheless, the definite structural transitions are believed to accompany the small-strain deformations. These transformations are likely in the partial loss of connectivity of clusters of stiff and viscous crystallites reminding the elastic percolation phenomenon. The stress induced destruction of narrow and therefore highly loaded bridges between neighbouring crystallites and/or inside crystallites should be a realistic reason for this transition. The local transformation of a small portion of stiff and plastic crystalline component (CC) into the soft and highly elastic amorphous component (AC): CC $\rightarrow$ AC, which entails loss of connectivity of crystalline domains, can alter mechanical response of semi-crystalline polymers even at small strains.

The paper is organized as follows. Experimental data on stress-strain diagrams of uniaxial tension for low density polyethylene (LDPE) and polypropylene (PP) will be demonstrated and discussed in Section 4. It will be shown that an irregular unloading behaviour is observed even in a limit of small deformations (the maximum strain does not exceed the yield point). To interpret and describe this phenomenon, three one-dimensional (1D) constitutive models are developed. Each of them takes into account a certain type of a strain-induced evolution of polymer structure and enables to provide sufficiently good fitting of the experimental diagrams.

The first model (Section 3.2.1) admits changes of the modulus, $E^{(\mathrm{cr})}$, and the plastic ability, $\chi^{(\mathrm{cr})}$ (the value inverse to viscosity, $\chi = 1/\eta$) of a CC. But this model does not include CC $\rightarrow$ AC transformation due to the strain-induced transformation of crystallites as well as links between them. Three negative consequences of this model will be demonstrated. The first one is in unrealistically large variations of $E^{(\mathrm{cr})}$ and $\chi^{(\mathrm{cr})}$ in a process of deformation, which arise with attempts to get a satisfactory description of experimental data. Second, fitting parameters are found to depend on maximum strain $\bar{\varepsilon}$ reminding features of the approaches discussed above. Third, the model predicts an essential drop of $E^{(\mathrm{cr})}$ contradicting the strain hardening of stretched polymers [4–9, 14, 15].

The second model (Section 3.2.1) includes the same constitutive equations for CC and AC as the first one but admits additionally the partial transformation of crystallites to amorphous phase. This transformation is assumed to result in change of crystallinity degree without qualitative modification in the morphology of crystallite clusters. The introducing of the strain induced local destruction of crystalline phase makes it possible to remove unrealistic diminution of $E^{(\mathrm{cr})}$ of the previous version. However, the other negative consequences still remain. In particular, the large decrease in the crystallinity degree should be assumed to get a sufficient fitting.

The evident progress in understanding of physical origin of non-conventional mechanical behaviour of semi-crystalline polymers is given by the third model (Section 3.2.2). The key point of this model is the assumption that the deformation induced transformation of CC results in the structural transition, which is in

a loss of connectivity in clusters of crystallites. It is shown that this constitutive approach is able to explain the observed small-strain loading-unloading behaviour of PP and LDPE with realistic evolution of mechanical and structural characteristics of these materials.

2. Experimental procedure

Isotactic polypropylene, PP, (Novolen 1100L) and low density polyethylene, LDPE, were supplied by BASF (Targor). ASTM dumbbell specimens were injection moulded with length 148 mm, width 13 mm and thickness 3.15 mm. Uniaxial tensile tests were performed at room temperature on a testing machine DELTALAB DN 30 equipped with electro-mechanical sensors for the control of longitudinal strains in the active zone of samples. The tensile force was measured by a standard load cell.

PP and LDPE specimens were stretched with a fixed cross-head velocity corresponded to initial strain rates $\dot{\varepsilon} = 8.3 \times 10^{-3}$ s^{-1} and $\dot{\varepsilon} = 5.7 \times 10^{-4}$ s^{-1}, respectively, up to the unloading strain, $\bar{\varepsilon}$, and then unloaded with the same cross-head speed to the zero stress. The chosen cross-head speeds ensure nearly isothermal experimental conditions.

Any series of experiments consisted of three-five tests with return strain values $\bar{\varepsilon} = 0.032$, 0.053, 0.072, 0.094 and 0.106 for PP and $\bar{\varepsilon} = 0.031$, 0.061 and 0.09 for LDPE. Each measurement was carried out on a new sample. The strains interval was chosen below the yield stresses, which are of the values $\varepsilon_y = 0.13$ and 0.12 for a PP and LDPE, respectively. Such interval can be regarded as small strain region.

3. Modelling of small-strain response of semi-crystalline polymers

3.1. Constitutive equation for crystalline and amorphous components

Multi dimensional constitutive modelling of semi-crystalline polymers is developed intensively recent years [see, for example, [4–9, 14–17]. The coupling between polymer texture and its mechanical response is one of the most important features of approaches proposed. The only one mode of deformation of PP and LDPE, namely the low rate uniaxial tension below the yield point, is analyzed in this paper. This mode is accompanied by orientation of crystallites, which, in turn, results in the strain hardening and diminution of plastic ability. In simplified 1D models reorientation processes will be taken into account just explicitly by introducing an increase of modulus, $E^{(cr)}$, along with decrease of plastic ability, $\chi^{(cr)}$, of crystallites in course of deformation. The rates of variation of these characteristics are supposed to be proportional to the stress applied to the crystallites:

$$\dot{E}^{(cr)} = k_E \sigma^{(cr)} E^{(cr)}, \tag{1}$$

$$\dot{\chi}^{(cr)} = -k_\chi \sigma^{(cr)} \chi^{(cr)}. \tag{2}$$

These rates are proportional to values of the corresponding parameters which ensure the expected tendencies in evolution of modulus and plastic ability along with conservation of their sign.

The small-strain limit justifies an additive representation of CC total strain, $\varepsilon^{(cr)}$, in terms of elastic, $\varepsilon_e^{(cr)}$, and plastic, $\varepsilon_p^{(cr)}$, components

$$\varepsilon^{(cr)} = \varepsilon_e^{(cr)} + \varepsilon_p^{(cr)}. \tag{3}$$

Particularly, Equation 3 prompts that the stress in the crystalline phase is produced only by elastic strain:

$$\sigma^{(cr)} = E^{(cr)} \varepsilon_e^{(cr)}, \tag{4}$$

The dependence of the plastic strain rate for CC upon the stress applied is also approximated by a linear law

$$\dot{\varepsilon}_p^{(cr)} = \chi^{(cr)} \sigma^{(cr)} \tag{5}$$

and is characterized by a plastic ability, $\chi^{(cr)}$.

Similarly to assumptions of [4–9, 14–17], the amorphous phase of SCP is supposed to be in a rubber-like state. It means that (i) elastic moduli of AC are much smaller than that of CC (Young modulus, particularly $E^{(am)} \ll E^{(cr)}$) and (ii) deformation is reversible in this phase. For the 1D version applied to a small strain case linear algebraic coupling

$$\sigma^{(am)} = E^{(am)} \varepsilon^{(am)} \tag{6}$$

serves as a constitutive approximation.

Equations 1–6 will be used to derive three constitutive models describing mechanical response of SCP in following sections.

3.2. Structural models and constitutive equations for semi-crystalline polymers

Obviously, the morphology of the SCP essentially determines its mechanical behaviour. Several realistic and hypothetic multidimensional structural models were suggested [16, 17] and their ability to simulate deformation behaviour of the material was analyzed. This study is restricted by the 1D approach. Nevertheless, certain important conclusions of the multidimensional representations are included into the present constitutive modelling.

3.2.1. The perfect mixture model

The coincidence of displacements and, hence, of total strains in crystalline and amorphous phases at each point is supposed in this approach:

$$\varepsilon = \varepsilon^{(am)} = \varepsilon^{(cr)} = \varepsilon_e^{(cr)} + \varepsilon_p^{(cr)}. \tag{7}$$

In the 1D version it can be represented as a parallel connection of c crystalline and $(1 - c)$ of amorphous elements (Fig. 2). The additive law for stresses

$$\sigma = c\sigma^{(cr)} + (1 - c)\sigma^{(am)}. \tag{8}$$

corresponds to this connection.

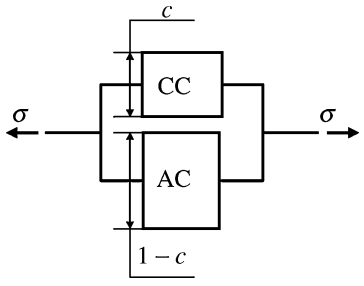

Figure 2 The 1D representation of a perfect mixture model. Widths of rectangular boxes depict volume fractions, c and $1 - c$, respectively.

The first constitutive model supposes to keep fixed the SCP structure, i.e., (i) the crystallinity degree, c, and (ii) a homogeneous distribution (perfect mixture) of crystalline and amorphous phases both at initial and deformed stages. Equations (1)–(8) form the system of constitutive relations:

$$\begin{cases} \dot{\varepsilon}_{\mathrm{e}}^{(\mathrm{cr})} = \dot{\varepsilon} - \chi^{(\mathrm{cr})} E^{(\mathrm{cr})} \varepsilon_{\mathrm{e}}^{(\mathrm{cr})}, \\ \dot{E}^{(\mathrm{cr})} = k_{\mathrm{E}} E^{(\mathrm{cr})} \varepsilon_{\mathrm{e}}^{(\mathrm{cr})}, \\ \dot{\chi}^{(\mathrm{cr})} = -k_{\chi} \chi^{(\mathrm{cr})} E^{(\mathrm{cr})} \varepsilon_{\mathrm{e}}^{(\mathrm{cr})}, \\ \sigma = cE^{(\mathrm{cr})} \varepsilon_{\mathrm{e}}^{(\mathrm{cr})} + (1-c) E^{(\mathrm{am})} \varepsilon, \end{cases} \quad \begin{cases} \varepsilon_{\mathrm{e}}^{(\mathrm{cr})}\big|_{\mathrm{t}=0} = 0, \\ E^{(\mathrm{cr})}\big|_{\mathrm{t}=0} = E_0^{(\mathrm{cr})}, \\ \chi^{(\mathrm{cr})}\big|_{\mathrm{t}=0} = \chi_0^{(\mathrm{cr})}. \end{cases} \tag{9}$$

The next approach is also based on the assumption of perfectly mixed components. It admits additionally the partial CC → AC transformation obviously accompanied by a decrease in a crystallinity degree c remaining in the framework of the same spatial arrangement of phases (the approximation of perfect mixture). The rate of a single crystallite transformation is supposed to be proportional to a stress applied. Thereby the kinetics of the transformation should be described as

$$\dot{c} = -k_{\mathrm{c}} \sigma^{(\mathrm{cr})} c. \tag{10}$$

Joining Equation 10 with the system (9) we obtain *the second constitutive model*:

$$\begin{cases} \dot{\varepsilon}_{\mathrm{e}}^{(\mathrm{cr})} = \dot{\varepsilon} - \chi^{(\mathrm{cr})} E^{(\mathrm{cr})} \varepsilon_{\mathrm{e}}^{(\mathrm{cr})}, \\ \dot{E}^{(\mathrm{cr})} = k_{\mathrm{E}} E^{(\mathrm{cr})} \varepsilon_{\mathrm{e}}^{(\mathrm{cr})}, \\ \dot{\chi}^{(\mathrm{cr})} = -k_{\chi} \chi^{(\mathrm{cr})} E^{(\mathrm{cr})} \varepsilon_{\mathrm{e}}^{(\mathrm{cr})}, \\ \dot{c} = -k_{\mathrm{c}} c E^{(\mathrm{cr})} \varepsilon_{\mathrm{e}}^{(\mathrm{cr})}, \\ \sigma = cE^{(\mathrm{cr})} \varepsilon_{\mathrm{e}}^{(\mathrm{cr})} + (1-c) E^{(\mathrm{am})} \varepsilon, \end{cases} \quad \begin{cases} \varepsilon_{\mathrm{e}}^{(\mathrm{cr})}\big|_{\mathrm{t}=0} = 0, \\ E^{(\mathrm{cr})}\big|_{\mathrm{t}=0} = E_0^{(\mathrm{cr})}, \\ \chi^{(\mathrm{cr})}\big|_{\mathrm{t}=0} = \chi_0^{(\mathrm{cr})}, \\ c|_{\mathrm{t}=0} = c_0. \end{cases} \tag{11}$$

3.2.2. Simulation of a connectivity transition

The gradual evolution both of mechanical and structural parameters of the materials can describe noticeable changes in a deformation response only being accompanied by noticeable changes of these parameters (see the next section). However, such changes are not realistic at small strain tests. The essential changes in properties can be caused by small variations of parameters only if these variations lead to qualitative transformations of morphology. Loss of connectivity by a cluster of crystallites as a result of rearrangement of CC seems to be the most realistic transition. In order to justify an alternative (to the second approach) way of the CC → AC transformation it makes sense to consider the chess-like disposition of crystallites surrounded by amorphous phase represented in (Fig. 3, see also [17]). The dark and light regions correspond to crystalline (CC) and amorphous (AC) components of SCP, respectively. The relative area of the dark regions coincides with the crystallinity degree, c.

CC → AC transformations are depicted in Fig. 3 by a simple diminution of crystallites dimensions ((a) → (b) and (c) → (d)). These two transformations differ in an initial crystallinity degree, c, and material geometry: SCP with disconnected crystallites is shown in Fig. 3a (low c) and a case of an existence of connected cluster of crystallites (sufficiently high c) corresponds to Fig. 3c. The second transformation, (c) → (d), in contrast to the first one is accompanied by the critical phenomenon: violation of connectivity of the crystallite cluster along the stretching direction.

Fig. 3e schematically reflects the fact that this percolation-like transition should occur in reality not by the simultaneous diminution of crystallites size, but by the destruction only of narrow and, hence, mostly stressed regions, surrounded on Fig. 3c by circles. CC → AC transformation of these regions also provides a similar disconnection effect, but by much less (compared to (d)) diminution in c.

Obviously, the chess-like representation of the structure is extremely simplified compared to realistic multi scale morphology of SCP. Nevertheless, this scheme includes two important advantages with respect to a perfect mixture model. The first one is simulation of spatial separation of crystalline and amorphous phases. The second is the ability of the chess-like model to take into account the connectivity of crystalline or amorphous components. The strong influence of this feature on the mechanical behaviour of heterogeneous media is qualitatively understandable and it was justified in numerous papers (see, for example, [18–20] devoted to elasticity of disordered discrete systems and [21, 22] for continuum composites). Actually, if a binary composite consists of randomly distributed stiff and soft elements (domains) then at small fraction c of the stiff regions they are disconnected and, hence, the soft-like response of the system takes place. On the contrary, the stiff-like behaviour is expected if c exceeds a percolation threshold c_{cr}.

In spite of that the chess-like model represents a regular structure, it also obeys the connectivity transition with the threshold $c_{\mathrm{cr}} = 0.5$: the crystallites are disconnected at $c < 0.5$ (see Fig. 3a, b and d), and connected if $c > 0.5$, (Fig. 3c). In the second perfect mixture model a stress-induced transformation of crystallites does not include violation of connectivity. This fact may be expressed in terms of the chess-like structure as (a) → (b) transformation of Fig. 3. It corresponds to the case of $c < c_{\mathrm{cr}}$ and takes into account just a diminution of crystallite sizes.

Our *third constitutive approach* includes transitions like (c) → (d) or (c) → (e) of Fig. 3. The essence of this

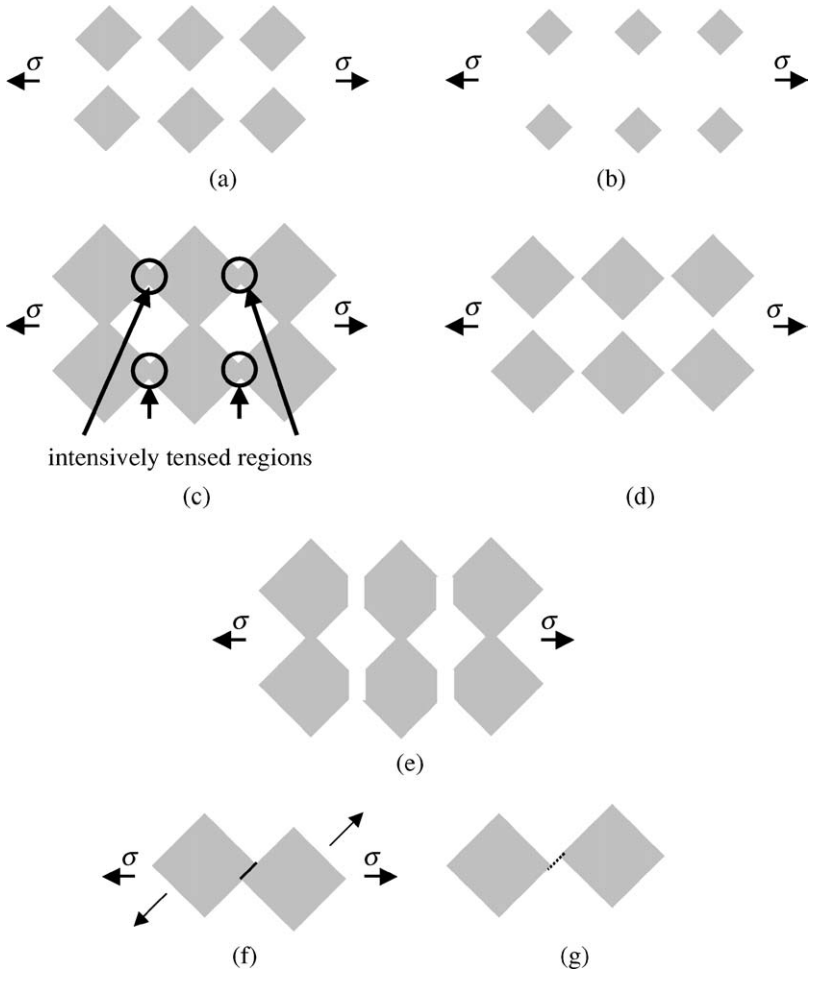

Figure 3 Schematic representation of a chess-like structure of SCP: the initial morphologies (a), (c), and (f) transform to the hypothetic structures (b), (d), (e) or (g) as a result of stress-induced transformation of crystallites (the dark regions).

model is in taking into account the loss of connectivity between crystallites. It becomes apparent with penetration of a newly formed amorphous phase (N) in the overstrained area between neighbouring crystallites. In the framework of the 1D approach this fact may be expressed as a serial CC-N connection shown in Fig. 4b and c.

In this paper we will not concern the phenomenon of strain recovering observed after unloading. This effect consists in almost complete elimination of the residual strains due to the elasticity of the amorphous phase and processes of recrystallization. It takes much more time compared to the duration of the loading-unloading experiment. In our 1D description this recovering is driven by the parallel AC element in Fig. 4b. Taking into account that the amorphous phase is a soft ($E^{(\mathrm{am})} \ll E^{(\mathrm{cr})}$) we may neglect it in simulation of loading-unloading processes within the third model. It simplifies calculations, which will be done in the framework of serial connection presented in Fig. 4c.

The serial connection of a newly formed portion, $(1-c)$, of amorphous component with the rest portion, c, of crystalline component requires the replacement of Equations 7 and 8 for strains and stresses, corresponded to a parallel connection, by the following ones:

$$\begin{aligned}\varepsilon &= c\varepsilon^{(\mathrm{cr})} + (1-c)\varepsilon^{(\mathrm{am})} \\ &= c\left(\varepsilon_{\mathrm{e}}^{(\mathrm{cr})} + \varepsilon_{\mathrm{e}}^{(\mathrm{am})}\right) + (1-c)\varepsilon^{(\mathrm{am})}, \qquad (12)\end{aligned}$$

$$\sigma = \sigma^{(\mathrm{cr})} = E^{(\mathrm{cr})}\varepsilon_{\mathrm{e}}^{(\mathrm{cr})} = \sigma^{(\mathrm{am})} = E^{(\mathrm{am})}\varepsilon^{(\mathrm{am})}. \qquad (13)$$

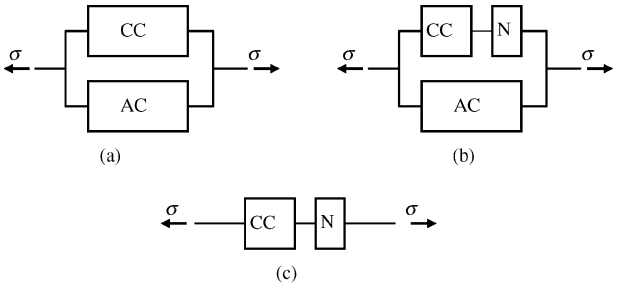

Figure 4 1D simulation of connectivity-disconnectivity transition in deformation process: (a) is the initial state of SCP with connected CC; (b) represents a newly formed amorphous phase N between neighbouring crystallites appearing during deformation; (c) is the simplified version of scheme (b) neglecting a parallel AC branch.

It gives the strain of amorphous part N and the plastic constituent of CC:

$$\varepsilon^{(\mathrm{am})} = \frac{E^{(\mathrm{cr})}}{E^{(\mathrm{am})}}\varepsilon_{\mathrm{e}}^{(\mathrm{cr})}, \qquad (14)$$

$$\varepsilon_{\mathrm{p}}^{(\mathrm{cr})} = \frac{1}{c}\varepsilon - \left(1 + \frac{1-c}{c}\frac{E^{(\mathrm{cr})}}{E^{(\mathrm{am}}}\right)\varepsilon_{\mathrm{e}}^{(\mathrm{cr})}. \qquad (15)$$

Differentiating Equation 15 and taking into account Equation 5 for the plastic strain rate of crystallites we obtain:

$$\dot{\varepsilon}_{\mathrm{p}}^{(\mathrm{cr})} = \chi^{(\mathrm{cr})} E^{(\mathrm{cr})} \varepsilon_{\mathrm{e}}^{(\mathrm{cr})} = \frac{\dot{\varepsilon}}{c} + \dot{c} \frac{E^{(\mathrm{cr})} \varepsilon_{\mathrm{e}}^{(\mathrm{cr})} - E^{(\mathrm{am})} \varepsilon}{c^2 E^{(\mathrm{am})}} - \dot{\varepsilon}_{\mathrm{e}}^{(\mathrm{cr})} \frac{(1-c)E^{(\mathrm{cr})} + cE^{(\mathrm{am})}}{cE^{(\mathrm{am})}} - \dot{E}^{(\mathrm{cr})} \frac{(1-c)\varepsilon_{\mathrm{e}}^{(\mathrm{cr})}}{cE^{(\mathrm{am})}} \tag{16}$$

Extracting the rate of elastic strain $\dot{\varepsilon}_{\mathrm{e}}^{(\mathrm{cr})}$ from Equation 16 and substituting it as the first equation of the system (11) along with the replacement of the last equation of (11) by the relation (13) for the stress we arrive to the 1D version of constitutive model including an idea of the strain-induced changes of connectivity of SCP morphology:

$$\begin{cases} \dot{\varepsilon}_{\mathrm{e}}^{(\mathrm{cr})} = \\ \quad \dfrac{\dot{\varepsilon} E^{(\mathrm{am})} + \frac{\dot{c}}{c}(E^{(\mathrm{cr})}\varepsilon_{\mathrm{e}}^{(\mathrm{cr})} - E^{(\mathrm{am})}\varepsilon) - \dot{E}^{(\mathrm{cr})}(1-c)\varepsilon_{\mathrm{e}}^{(\mathrm{cr})} - \chi^{(\mathrm{cr})} E^{(\mathrm{cr})} E^{(\mathrm{am})} c \varepsilon_{\mathrm{e}}^{(\mathrm{cr})}}{(1-c)E^{(\mathrm{cr})} + cE^{(\mathrm{am})}}, \\ \dot{E}^{(\mathrm{cr})} = k_E E^{(\mathrm{cr})} \varepsilon_{\mathrm{e}}^{(\mathrm{cr})}, \\ \dot{\chi}^{(\mathrm{cr})} = -k_\chi E^{(\mathrm{cr})} \varepsilon_{\mathrm{e}}^{(\mathrm{cr})}, \\ \dot{c} = -k_{\mathrm{c}} c E^{(\mathrm{cr})} \varepsilon_{\mathrm{e}}^{(\mathrm{cr})}, \\ \sigma = \sigma^{(\mathrm{cr})} = E^{(\mathrm{cr})} \varepsilon_{\mathrm{e}}^{(\mathrm{cr})} \end{cases} \tag{17}$$

(the initial conditions are the same as in (11)).

4. Results and discussion

The experimental stress-strain diagrams of the low rate tension and unloading of PP and LDPE are represented in Figs 5 and 6, respectively. The PP is more rigid than LDPE showing the larger level of stresses at the same strain values. From these data we can see that both of the polymers demonstrate series of common features. Primary it concerns unexpectedly small slopes of unloading branches of the diagrams along with values of residual strain compared to those predicted by conventional models (see also Fig. 1). The analysis of this phenomenon is carried out here on the basis of three constitutive models proposed in the previous section.

The first evaluation of fitting of experimental data shows that the first and the second models lead to the almost coincident curves, which are not distinguishable in Figs 5a and 6a. The third constitutive model provides the noticeably better fitting (Figs 5b and 6b) followed by a physically reasonable changing of polymer characteristics (see below). The results were found to provide the same peculiarities for PP and LDPE. We restrict further discussion by polypropylene only. The corresponding plots are given in Figs 7–9.

The variations of relative Young modulus $E^{(\mathrm{cr})}/E_0^{(\mathrm{cr})}$ of the crystalline component of PP in of loading-unloading processes, given by the first constitutive model, are represented in Fig. 7 ($E_0^{(\mathrm{cr})}$ is the initial value of the modulus). Recall that this approach supposes stability of morphology of semi-crystalline polymer and, hence, conservation of crystallinity degree c during deformation. Analysis of these plots reveals three non-realistic features inhere in the first model.

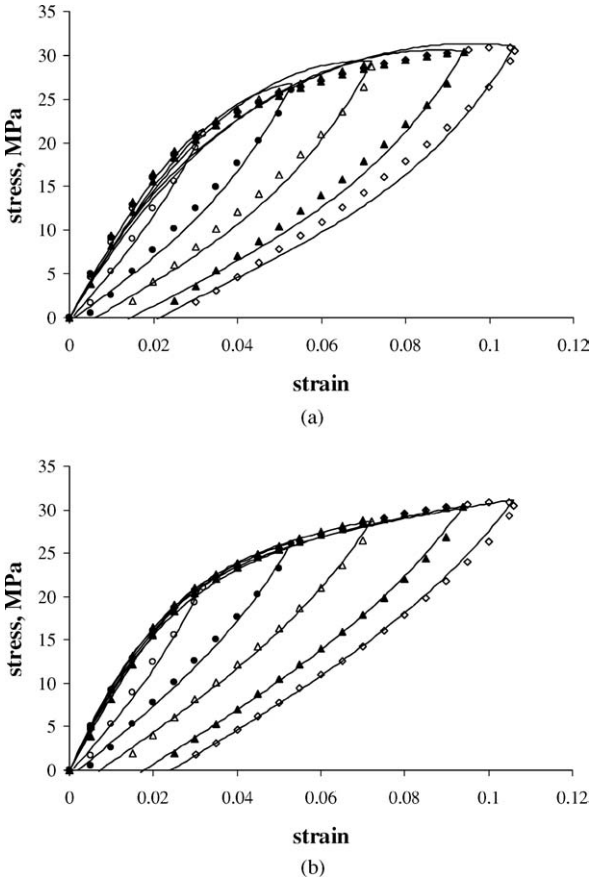

Figure 5 Experimental and theoretical loading-unloading stress-strain diagrams of PP at the fixed strain rate ($\dot{\varepsilon} = 8.27 \times 10^{-3}\ \mathrm{s}^{-1}$) for different values of the returned points ($\bar{\varepsilon} = 0.032$ (○); $\bar{\varepsilon} = 0.054$ (●); $\bar{\varepsilon} = 0.072$ (△); $\bar{\varepsilon} = 0.094$ (▲); $\bar{\varepsilon} = 0.106$ (∗)): (a) fitting with the first and second constitutive models, (b) fitting with the third constitutive model. The tests were carried out at room temperature.

1. In order to reach an acceptable fitting of the experimental data this model provides a great variation in the modulus (about five times for $\bar{\varepsilon} = 0.106$). The plastic ability of CC is found to change even more (we do not present these curves here to save a space). These results could not be accepted because of their unphysical content: it is hardly believed that the small-strain deformations could result in so great variations in a polymer texture and, hence, in material characteristics.

2. The material's parameters should not depend on the returned point, $\bar{\varepsilon}$. However, Fig. 7 clearly indicates that the first model possesses this unrealistic feature.

3. The uniaxial tension should induce orientation of crystallites in the drawing direction. At least it should cause the strain hardening of SCP [4–9, 14, 15]. But Fig. 7 demonstrates an opposite behaviour of the Young modulus. This contradiction follows from the attempt to get fitting (Fig. 5a) of the abnormally low slopes of the unloading branches of the experimental stress-strain diagrams under the assumption of the fixed morphology. As a result it gives a diminution of effective elastic modulus of CC.

The second constitutive approach is free from the last defect. It admits variation in SCP morphology due to the stress-induced transformation of crystallites. Including this feature (see Equation 7) into the constitutive model

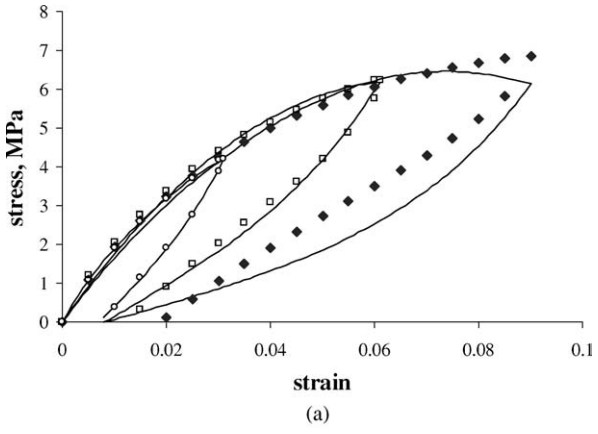

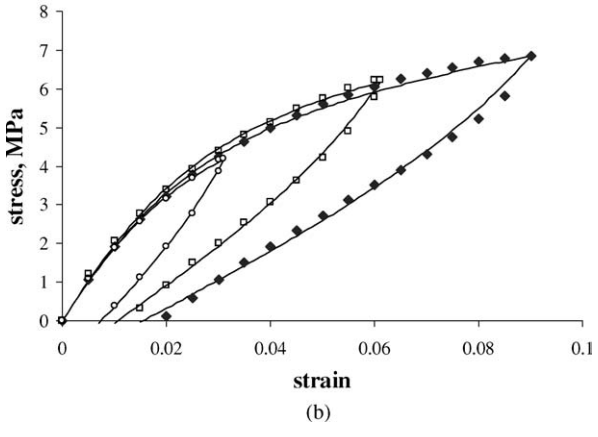

Figure 6 Experimental and theoretical loading-unloading stress-strain diagrams of LDPE at fixed strain rate ($\dot{\varepsilon} = 5.66 \times 10^{-4}\ s^{-1}$) for different values of the returned points ($\bar{\varepsilon} = 0.031$ (○); $\bar{\varepsilon} = 0.061$ (●); $\bar{\varepsilon} = 0.09$ (△)): (a) fitting with the first and second constitutive models, (b) fitting with the third constitutive model. The tests were carried out at room temperature.

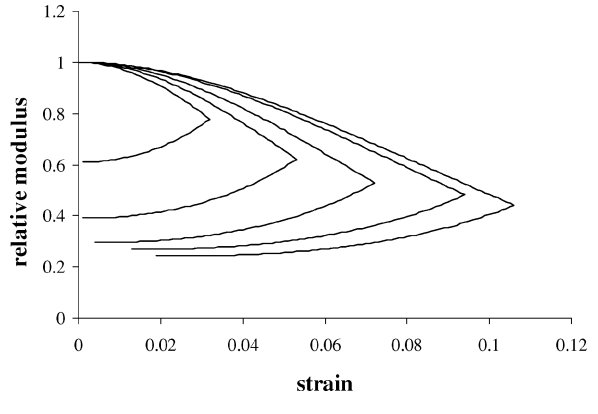

Figure 7 Relative Young moduli $E^{(cr)}/E_0^{(cr)}$ of PP crystallites predicted by the first constitutive model as functions of tensile strain at loading and unloading. The curves correspond to the same returned strains $\bar{\varepsilon}$ as in Fig. 5.

(Equations 11) makes it possible to compensate the decrease in the effective modulus by transformation of the stiff crystallites into the soft amorphous component. As a consequence of this modification, the Young modulus $E^{(cr)}$ of CC can be kept fixed or even slightly growing at tension. We do not show this plot because variation is small and is not seen.

The variations of relative material parameters $\chi^{(cr)}/\chi_0^{(cr)}$ and c/c_0, predicted by the second constitutive model, are shown in Fig. 8 ($\chi_0^{(cr)}$ and c_0 are the initial value of plastic ability and the crystallinity degree).

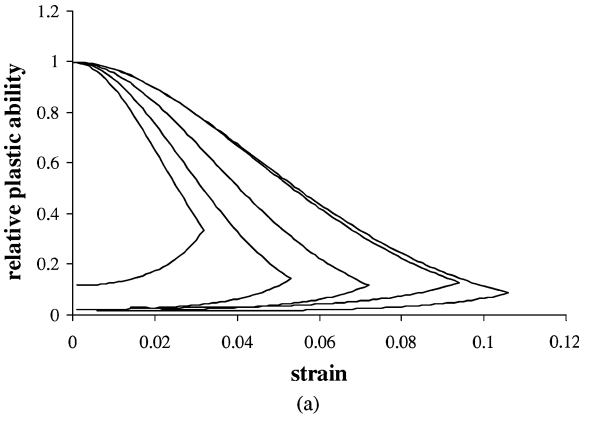

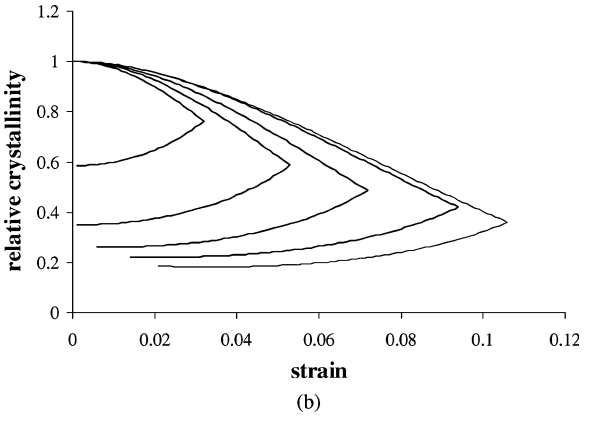

Figure 8 Variations of material parameters of PP crystallites predicted by the second constitutive model as a functions of tensile strain at loading and unloading: (a) relative plastic ability, $\chi^{(cr)}/\chi_0^{(cr)}$, (b) relative crystallinity degree c/c_0. The curves correspond to the same returned strains $\bar{\varepsilon}$ as in Fig. 5.

Diminution in these characteristics with deformation coincides qualitatively with the anticipated regularities of strain-induced evolution of the SCP texture. Nevertheless, the second model also demonstrates the rest of drawbacks listed above. First, the changes of these parameters are incredibly large for a small strain limit. Second, the results given by this model are still dependent on the strain $\bar{\varepsilon}$ at the returned point.

In contrast to the second approach, the third constitutive model takes into account penetration of the newly formed amorphous phase between the neighbouring crystallites. This serial connection (Fig. 4c) reflects the loss of connectivity in the crystallite clusters. The application of this model gives the appreciably better fitting of experimental data (see Fig. 5b) followed by variations in relative plastic ability $\chi^{(cr)}/\chi_0^{(cr)}$ and crystallinity degree c/c_0 shown in Fig. 9.

The obtained results demonstrate undoubtedly that the third constitutive approach, supposing the loss of connectivity by crystalline component t is much more successful than the previous ones. The excellent fitting is obtained along with a slight increase in crystallite elastic modulus. The plastic ability (Fig. 9a) and the degree of crystallinity (Fig. 9b) exhibit relatively small diminution. It is seen from these figures that the calculated parameters are almost independent of position of the returned point, $\bar{\varepsilon}$: the unique variation of the material characteristics is obtained on the basis of the third constitutive model.

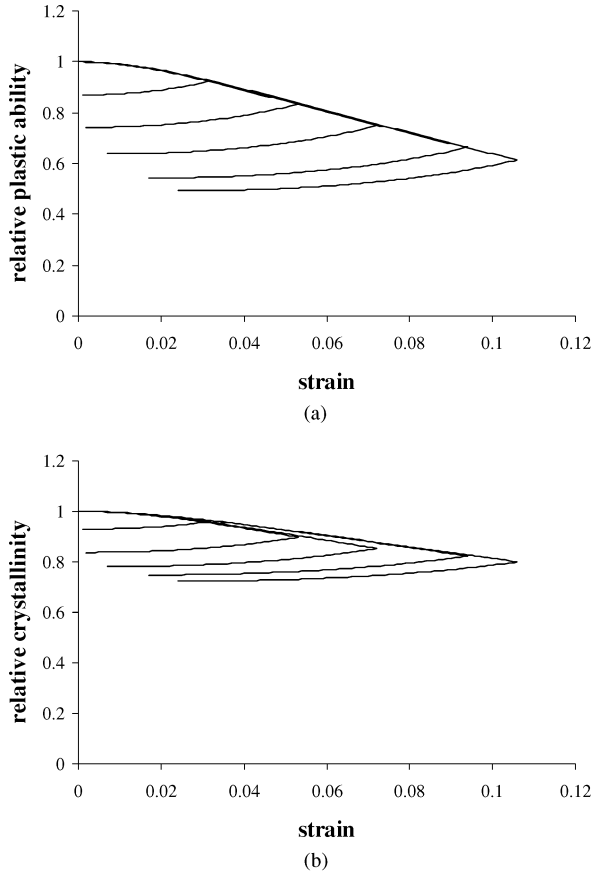

Figure 9 Variations of material parameters of PP crystallites predicted by the third constitutive model as a functions of tensile strain at loading and unloading: (a) relative plastic ability $\chi^{(cr)}/\chi_0^{(cr)}$, (b) relative crystallinity degree c/c_0. The curves correspond to the same returned strains $\bar{\varepsilon}$ as in Fig. 5.

This important result is supplied by the physical understanding of the observed phenomenon. Emphasise that it is caused exclusively due to critical changes in SCP topology resulting connectivity-disconnectivity transitions. We claim that the experimentally found effects of unconventional unloading behaviour of PP and LDPE under the small-strain deformations cannot be understood without taking into account the critical changes in the structure.

5. Conclusions

The unconventional loading-unloading behaviour of PP and LDPE below the yield point was experimentally found. The essence of the phenomenon is in low slopes of unloading portions of deformation diagrams and values of residual strains. These observations point that certain evolution of polymer morphology accompanies the drawing process. Otherwise one would expect the linear viscoelastic response of semi-crystalline polymers in a limit of small strains.

Three structure sensitive constitutive approaches are developed and analyzed for the understanding of the phenomenon. Each of them considers semi-crystalline polymer as a binary blend of crystalline and amorphous components. The mixture of these components is supposed to be perfect in the first and second models. On the contrary, phases are assumed to occupy separated domains in the third approach. Connectivity of these domains can be violated in a deformation process.

We assumed that reversible elastic constitutive relations describe mechanical response of the amorphous component. The crystallites are much stiffer and capable for the plastic deformation and reorientation. It leads to a strain hardening and decreasing in plastic ability under uniaxial drawing.

In contrast to the first model, the second and third ones admit stress-induced CC $\rightarrow$ AC transformation. The difference between these approaches implies that the second model is restricted by the conservation of spatial morphology of SCP (perfect mixture) while the third one takes into account loss of connectivity in crystallite clusters.

It is found that a reasonable fitting of the stress-strain diagrams can be obtained with each approach (the best one is obtained by the third model). However, the physically admissible variations of mechanical (elastic modulus and plastic ability of crystallites) and structural (crystallinity degree) characteristics, necessary for a good fitting, are achieved only in the case when the connectivity transitions are admitted. The variations predicted by the first and second models are too large to be considered as realistic ones at small deformations. Moreover, they are dependent of the values of return strains. The first approach also leads to a diminution of crystallite elastic modulus at drawing, which contradicts with the well-known phenomenon of the strain hardening.

We conclude the paper by the following remark. It is very important to develop the proposed constitutive models by 2D and 3D simulations. The 1D version is restricted by a uniform diminution of crystalline domains starting from the CC – AC interface (transformations (a) $\rightarrow$ (b), (c) $\rightarrow$ (d) are shown in Fig. 3 by simultaneous diminution in the crystallites sizes). Such uniformity is caused by the same stress condition for every crystallite, which is provided by a one-dimensional simulation. Actually, the local transformation of overstrained narrow regions of crystallites ((c) $\rightarrow$ (e) transformation in Fig. 3) seems to be much more realistic. Such transformation implies a connectivity transition, caused by a very small change in c, even smaller than that found by the third approach of a given simulation. All the technique and algorithms are already developed (see [17]) and the mentioned multidimensional simulation will be performed in the nearest future. Loss of crystalline connectivity can also occur following the mechanism of local crystallographic slip (Fig. 3f and g). Its realization does not require any change in c at all.[1]

Appendix: Algorithm of the fitting procedure

Fitting of measured stress-strain diagrams was performed using the unique algorithm for every approach, including the formal description on the basis of Maxwell viscoelastic element in Fig. 1.

[1]The last mechanism of the loss of crystal connectivity was proposed by the Referee of the paper. Authors are greatly thankful him for this advise.

The algorithm of fitting is based on the following procedure. The experimental data are given by a set of $n^{(\mathrm{ex})}$ points, $(\varepsilon_{\mathrm{j}}^{(\mathrm{ex})}, \sigma_{\mathrm{j}}^{(\mathrm{ex})})$ on the strain-stress plane ($j = 1, 2, \ldots, n^{(\mathrm{ex})}$). Stress values at same strains, $\sigma_{\mathrm{j}}^{(\mathrm{th})} = \sigma^{(\mathrm{th})}(\varepsilon_{\mathrm{j}}^{(\mathrm{ex})})$ can be calculated using one or other model. Particularly, well-known analytical formula

$$\sigma^{(\mathrm{th})}(\varepsilon) = \bar{\sigma}\exp\left(-\frac{p_1}{p_2\dot{\varepsilon}}(\varepsilon-\bar{\varepsilon})\right) + \eta\dot{\varepsilon}\left(1-\exp\left(-\frac{p_1}{p_2\dot{\varepsilon}}(\varepsilon-\bar{\varepsilon})\right)\right) \quad (18)$$

where parameters correspond to the stiffness, $p_1 = E$, and viscosity, $p_2 = \eta$, of the Maxwell element; $(\bar{\varepsilon}, \bar{\sigma})$ is the given point of the strain-stress curve (for example, the return point); $\dot{\varepsilon}$ is a fixed strain rate.

In the case of the constitutive equations considered in the paper the values of $\sigma_{\mathrm{j}}^{(\mathrm{th})}$ depend on a larger number of material parameters. For the first model we have: $p_1 = E_0^{(\mathrm{cr})}$, $p_2 = E^{(\mathrm{am})}$, $p_3 = \chi_0^{(\mathrm{cr})}$, $p_4 = k_{\mathrm{E}}$, $p_5 = k_\chi$. In the case of the second and third ones two parameters, $p_6 = c_0$, and $p_7 = k_c$, should be added to this set. These parameters, $p_1, p_2, \ldots, p_{\mathrm{m}}$, were seeking from the condition of minimum of the square deviation between theoretical and experimental stresses:

$$U = \sum_{\mathrm{j}}\left(\sigma_{\mathrm{j}}^{(\mathrm{th})} - \sigma_{\mathrm{j}}^{(\mathrm{ex})}\right)^2. \quad (19)$$

The following iteration procedure was used to fulfill this condition. The calculated stresses $\sigma_{\mathrm{j}}^{(\mathrm{th})}$ and, hence, the square deviation U, are the functions of the seeking parameters:

$$U = U(p_1, p_2, \ldots, p_{\mathrm{m}}) = \sum_{\mathrm{j}}\left(\sigma_{\mathrm{j}}^{(\mathrm{th})}(p_1, p_2, \ldots, p_{\mathrm{m}}) - \sigma_{\mathrm{j}}^{(\mathrm{ex})}\right)^2. \quad (20)$$

An key point of the iteration procedure consists in the replacement of the function $U(p_1, p_2, \ldots, p_{\mathrm{m}})$ by its expansion $\tilde{U}(p_1, p_2, \ldots, p_{\mathrm{m}})$ in the Taylor series up to squire terms:

$$\begin{aligned} U(p_1, p_2, \ldots, p_{\mathrm{m}}) &\approx \tilde{U}(p_1, p_2, \ldots, p_{\mathrm{m}}) \\ &= U\left(p_1^{(\mathrm{s})}, p_2^{(\mathrm{s})}, \ldots, p_{\mathrm{m}}^{(\mathrm{s})}\right) \\ &\quad + \sum_{\mathrm{k}}\frac{\partial U\left(p_1^{(\mathrm{s})}, p_2^{(\mathrm{s})}, \ldots, p_{\mathrm{m}}^{(\mathrm{s})}\right)}{\partial p_k}\left(p_{\mathrm{k}} - p_{\mathrm{k}}^{(\mathrm{s})}\right) \\ &\quad + \frac{1}{2}\sum_{k,l}\frac{\partial^2 U\left(p_1^{(\mathrm{s})}, p_2^{(\mathrm{s})}, \ldots, p_m^{(\mathrm{s})}\right)}{\partial p_{\mathrm{k}}\partial p_{\mathrm{l}}} \\ &\quad \times\left(p_{\mathrm{k}} - p_{\mathrm{k}}^{(\mathrm{s})}\right)\left(p_{\mathrm{l}} - p_{\mathrm{l}}^{(\mathrm{s})}\right) \end{aligned} \quad (21)$$

Each iteration step $(p_1^{(\mathrm{s})}, p_2^{(\mathrm{s})}, \ldots, p_{\mathrm{m}}^{(\mathrm{s})}) \to (p_1^{(\mathrm{s}+1)}, p_2^{(\mathrm{s}+1)}, \ldots, p_{\mathrm{m}}^{(\mathrm{s}+1)})$ was made by solving the system of linear algebraic equations corresponding to the zero gradient of $\tilde{U}(p_1, p_2, \ldots, p_{\mathrm{m}})$:

$$\begin{aligned} &\sum_{\mathrm{l}}\frac{\partial^2 U\left(p_1^{(\mathrm{s})}, p_2^{(\mathrm{s})}, \ldots, p_{\mathrm{m}}^{(\mathrm{s})}\right)}{\partial p_{\mathrm{k}}\partial p_{\mathrm{l}}}p_{\mathrm{l}}^{(\mathrm{s}+1)} \\ &\quad = \sum_{\mathrm{l}}\frac{\partial^2 U\left(p_1^{(\mathrm{s})}, p_2^{(\mathrm{s})}, \ldots, p_{\mathrm{m}}^{(\mathrm{s})}\right)}{\partial p_{\mathrm{k}}\partial p_{\mathrm{l}}}p_{\mathrm{l}}^{(\mathrm{s})} \\ &\qquad - \frac{\partial U\left(p_1^{(\mathrm{s})}, p_2^{(\mathrm{s})}, \ldots, p_{\mathrm{m}}^{(\mathrm{s})}\right)}{\partial p_{\mathrm{k}}}. \end{aligned} \quad (22)$$

The initial values $(p_1^{(0)}, p_2^{(0)}, \ldots, p_{\mathrm{m}}^{(0)})$ of the material parameters were chosen as close as possible to the seeking minimum.

If $\sigma^{(\mathrm{th})}$ is represented analytically (Equation 18), the first and second derivatives of $U(p_1, p_2, \ldots, p_{\mathrm{m}})$ figuring in Equation 22 can be calculated directly. But it is not the case of systems of constitutive Equations 10, 11 and 17. The stresses corresponding to these models (the last relation of systems (10), (11) and (17), respectively) depend on the set of parameters in two ways, explicitly and implicitly: $\sigma_{\mathrm{j}}^{(\mathrm{th})} = \sigma_{\mathrm{j}}^{(\mathrm{th})}(p_1, \ldots p_{\mathrm{m}}; y_1, \ldots y_{\mathrm{n}})$. The implicit dependence is given through $y_1 = \varepsilon_{\mathrm{e}}^{(\mathrm{cr})}$, $y_2 = E^{(\mathrm{cr})}$, $y_3 = \chi^{(\mathrm{cr})}$ and $y_4 = c$, which will be called further as state functions. y_4 is not included into the system (10), because the structure is supposed to be fixed in the corresponding model. So, we have $n = 3$ for the first approach and $n = 4$ for the second and the third ones. The state functions can be found only by numerical integration of corresponding systems of ordinary differential equations.

In turn, the state functions depend upon the seeking parameters $p_1, p_2, \ldots, p_{\mathrm{m}}$ by two different ways, which do not intersect. That is why the total set of parameters can be divided into two groups. For the first group the way is defined by an explicit and implicit dependence of the right-hand sides of differential equations:

$$\dot{y}_{\mathrm{l}} = f_{\mathrm{l}}(p_1, \ldots p_{\mathrm{m}}; y_1, \ldots y_{\mathrm{n}}). \quad (23)$$

It is a case of the parameters $p_4 = k_{\mathrm{E}}$ and $p_5 = k_\chi$. Quantities, which determine initial values of state functions, $p_1 = E_0^{(\mathrm{cr})}$, $p_3 = \chi_0^{(\mathrm{cr})}$, and $p_6 = c_0$, form the second group.

Algorithm of minimization supposes unique type of seeking parameters. That is why the parameters of the second group (let us keep in mind one of them, $p_{\mathrm{r}} = y_{\mathrm{q}}|_{t=0}$, for instance) were transformed into the first group in the result of the replacement of the corresponding state function, y_{q}, by the relative value, $\hat{y}_{\mathrm{q}}$:

$$y_{\mathrm{q}} \to \hat{y}_{\mathrm{q}} = \frac{y_{\mathrm{q}}}{p_{\mathrm{r}}}. \quad (24)$$

The new state function satisfies the fixed initial condition and new right-hand side of the differential equation

becomes dependent of p_r:

$$\left(\frac{dy_q}{dt} = f_q,\ y_q|_{t=0} = p_r\right) \rightarrow \left(\frac{d\hat{y}_q}{dt} = \hat{f}_q = \frac{f_q}{p_r},\ .\hat{y}_q|_{t=0} = 1\right). \quad (25)$$

First, $y_{ki} = \partial y_k \partial y_k / \partial p_i$, and second, $y_{kij} = \partial y_k / \partial p_i \partial p_j$ derivatives of the state functions, $y_1, \ldots, y_n$, were included into the corresponding system of differential equations:

$$\dot{y}_{ki} = f_{ki} = \frac{\partial f_k}{\partial p_i} + \sum_s \frac{\partial f_k}{\partial y_s} y_{si},$$

$$\dot{y}_{kij} = f_{kij} = \frac{\partial^2 f_k}{\partial p_i \partial p_j} + \sum_{s,t} \frac{\partial^2 f_k}{\partial y_s \partial y_t} y_{si} y_{tj} + \sum_s \left(\frac{\partial^2 f_k}{\partial p_i \partial y_s} y_{sj} + \frac{\partial^2 f_k}{\partial p_j \partial y_s} y_{si} + \frac{\partial f_k}{\partial y_s} y_{sij}\right) \quad (26)$$

with the zero initial conditions. The extended systems were integrated numerically by Runge-Kutta method and calculated values of the state functions and their derivatives were substituted into Equation 22.

Acknowledgments

Authors thank Mr. R. Beiber for accurate performance of series of measurements. Authors are greatly thankful to Prof. S. Ahzi for fruitful discussions. V. Oshmyan and S. Patlazhan appreciate administration and staff of the Institute of Mechanics of Fluids and Solids (IMFS) and of University of Louis Pasteur of Strasbourg for the excellent work conditions and assistance during their stay in IMFS in 2003. The work was partially supported by the Russian Foundation of Basic Research (Grant nos.: 03-03-32018 and 01-03-32237)

References

1. R. J. ASARO and A. NEEDELMAN, *Acta Metall.* **33** (1985) 923.
2. S. NEMAT-NASSER, in "Plasticity Today Modelling, Methods and Applications," edited by A. Sawczuk and G. Bianchi (Elsevier, 1985) p. 85.
3. M. R. RUBIN, *Int. J. Solids Struct.* **31** (1994) 2615.
4. Z. BARTCZAK, A. S. ARGON and R. E. COHEN, *Polymer* **35** (1994) 3427.
5. Z. BARTCZAK, R. E. COHEN and A. S. ARGON, *Macromolecules* **25** (1992) 4692.
6. Z. BARTCZAK, A. S. ARGON and R. E. COHEN, *ibid.* **25** (1992) 5036.
7. A. GALESKI, Z. BARTCZAK, A. S. ARGON and R. E. COHEN, *ibid.* **25** (1992) 5705.
8. B. J. LEE, A. S. ARGON, D. M. PARKS, S. AHZI and Z. BARTCZAK, *Polymer* **34** (1993) 3555.
9. B. J. LEE, D. M. PARKS and S. AHZI, *J. Mech. Phys. Solids* **41** (1993) 1651.
10. Y. REMOND, in Proceedings of the 13rd National Conference on Composites, Vol. 1, Strasbourg, March 2003, edited by Y. Rémond and J. Lamon, p. 503.
11. *Idem.*, *Comp. Sci. Techn.* (2003) in press.
12. A. D. DROZDOV and J.DEC. CHRISTIANSEN, *Europ. Polym. Journal* **39** (2003) 21.
13. *Idem.*, *Mech. Res. Commun.* (2003) in press.
14. V. G. OSHMYAN, *Polym. Sci.* B **37** (1995) 17.
15. K. P. HERRMANN, V. G. OSHMYAN, S. A. TIMAN and M. Y. SHAMAEV, *ibid.* C**44** (2002) 63.
16. J. A. W. VAN DOMMELEN, D. M. PARKS, M. C. BOYCE, W. A. M. BREKELMANS and F. P. T. BAAIJENS, *J. Mech. Phys. Solids* **51** (2003) 519.
17. V. G. OSHMYAN, S. A. TIMAN and M. Y. SHAMAEV, *Polym. Sci.* (2003) in press.
18. S. FENG and P. N. SEN, *Phys. Rev. Lett.* **52** (1984) 216.
19. Y. KANTOR and I. WEBMAN, *ibid.* **52** (1984) 1891.
20. M. SAHIMI and S. ARBABI, *Phys. Rev.* B **47** (1993) 703.
21. S. A. TIMAN and V. G. OSHMYAN, in Proceedings of the Fall Meeting of the Materials Research Society (MRS, Pittsburgh, 1994).
22. V. G. OSHMYAN, S. A. PATLAZHAN and S. A. TIMAN, *Phys. Rev.* E **64** (2001) 056108-1.

Received 13 August 2003
and accepted 3 March 2004